



Schweizerische Eidgenossenschaft  
Confédération suisse  
Confederazione Svizzera  
Confederaziun svizra

Eidgenössisches Departement für  
Umwelt, Verkehr, Energie und Kommunikation UVEK  
**Bundesamt für Energie BFE**

**Schlussbericht** November 2011

---

## **PECHOUSE**

**A COMPETENCE CENTER DEVOTED TO THE  
PHOTOELECTROCHEMICAL SPLITTING OF  
WATER AND PRODUCTION OF HYDROGEN**

---

**Auftraggeber:**

Bundesamt für Energie BFE  
Forschungsprogramm Brennstoffzellen und Wasserstoff  
CH-3003 Bern  
[www.bfe.admin.ch](http://www.bfe.admin.ch)

**Auftragnehmer:**

Ecole Polytechnique Fédérale de Lausanne  
EPFL SB ISIC LPI  
CH G1 526 (Bât. CH)  
Station 6  
CH-1015 Lausanne, Switzerland  
<http://pechouse.epfl.ch>

**Autoren:**

S. David Tilley  
Kevin Sivula  
Scott C. Warren  
Adriana Paracchino  
Maurin Cornuz  
Florian Le Formal  
Jérémie Brillet  
Michael Grätzel [Michael.graetzel@epfl.ch](mailto:Michael.graetzel@epfl.ch)  
Massimiliano Capezzali  
Hans B. Püttgen

**BFE-Bereichsleiter:** Dr. Stefan Oberholzer

**BFE-Programmleiter:** Dr. Stefan Oberholzer

**BFE-Vertrags- und Projektnummer:** 152933 / 102326

Für den Inhalt und die Schlussfolgerungen sind ausschliesslich die Autoren dieses Berichts verantwortlich.

## Abstract

PECHouse, the photoelectrochemistry centre of competence at the Swiss Federal Institute of Technology of Lausanne (EPFL), has been established to advance the technology of semiconductor-based photoelectrochemical (PEC) water splitting to produce H<sub>2</sub> and O<sub>2</sub> using sunlight as the energy input. The overall objective of the research is to design and develop novel semiconductor-based materials capable of harvesting and converting solar energy into chemical energy by oxidation of water into oxygen and reduction into hydrogen. Since its inception in September 2007, PECHouse research activities have centered on assembling tools and techniques for the development of the next generation of photoelectrochemical technology, alongside furthering the development of the state-of-the-art  $\alpha$ -Fe<sub>2</sub>O<sub>3</sub> photoanodes conceived at EPFL. Here we present the results from 2011 on our recent research accomplishments. Specifically, for WP1 we present results of new world-record benchmark photocurrent performance with colloidal Fe<sub>2</sub>O<sub>3</sub> photoanodes. Further, we present a study of surface treatments that affect the overpotential as well as plateau photocurrents. For WP2, progress in development of the host/guest approach for photoanodes is presented. Finally, we report breakthrough results on the photoactivity and stability of a Cu<sub>2</sub>O photocathodes for hydrogen production. Key data from previous years are summarized throughout this final report to give an overview of the entire PECHouse project.

## Buts du projet

As the world's supply of fossil fuels declines, hydrogen has become the most promising alternative fuel for the new energy economy. Hydrogen can be produced from various sources; however, hydrogen production from renewable sources is highly attractive. The most important renewable source of energy is the Sun, which shines in 10 minutes on planet Earth an amount of energy equal to the total yearly human consumption, yet we harness less than 2% of the world's energy demand due to a lack of suitable materials. PECHouse has been established as a centre of competence based at the *Swiss Federal Institute of Technology of Lausanne* (EPFL), in order to foster world-class research activities for semiconductor-based photoelectrochemical (PEC) water splitting into  $H_2$  and  $O_2$  using sunlight as the energy input.

PECHouse was established in September 2007 with three separate but related work-plans (WPs). The overall objective of the research is to design and develop novel semiconductor based materials capable of harvesting and converting solar energy into chemical energy by oxidation of water into oxygen and hydrogen. The first work plan (WP-1) extends continuing efforts on nanostructured iron oxide ( $Fe_2O_3$ ) photoanodes developed at EPFL's Laboratory of Photonics and Interfaces (LPI).<sup>1-4</sup> As stated in the Rapport annual 2010, our work with regard to WP-1 for 2011 focused on understanding the limitations at the surface that result in the high overpotential as well as to increase further the photocurrent of the hematite photoanodes. For the second work plan (WP-2), we have developed a conductive substrate for the host-guest approach. We have also achieved a major advance in stability of the  $Cu_2O$  photocathode material and investigated many different facets of the overlayer protection strategy.

## Travaux effectués et résultats acquis

### WP-1: $\alpha-Fe_2O_3$ Photoanodes

Following the previously reported success of applying  $IrO_2$  nanoparticles to the surface of our mesostructured  $Fe_2O_3$  created by APCVD (see 2009 report), we continued to investigate this system to gain further understanding. In particular, we investigated the deposition conditions which led to the increased performance. Using an extensive X-ray diffraction study we found that the state-of-the-art performance, which had been obtained through the reduction of precursor gas residence time, was explained by an enhanced preferential orientation of the highly conductive crystal planes perpendicular to the electron-collecting substrate. This result is presented in detail in a publication for a special issue regarding hydrogen of the journal entitled "Chemical Vapor Deposition."<sup>5</sup>

The enhanced performance allowed even better performance of the  $IrO_2$  modified  $Fe_2O_3$  photoanodes. The best performance recorded at 1.23 V vs. RHE is now  $3.3 \text{ mA cm}^{-2}$  under standard illumination conditions (See Figure 1), upon correcting the resistance losses within the cell (i.e. assessing the  $Fe_2O_3$  only). The total possible photocurrent delivered by this photoanode is close to  $4 \text{ mA cm}^{-2}$  before the onset of the dark current.

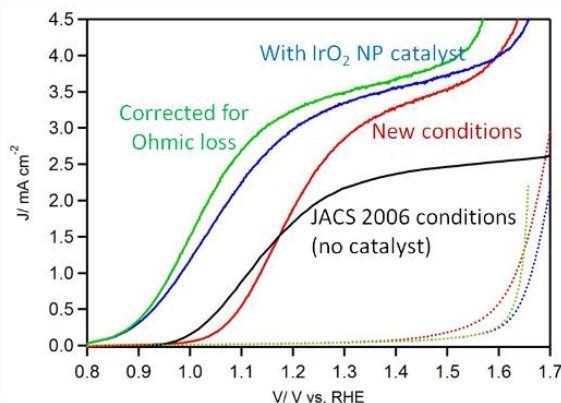


**Figure 1.** Photocurrent curves of  $IrO_2$ -modified  $Fe_2O_3$  prepared with APCVD at  $6 \text{ L min}^{-1}$  carrier gas flow rate. The black curve represents the photocurrent delivered by photoanodes prepared in 2006 ( $2 \text{ L min}^{-1}$ ), and the red curve shows the effect of the higher carrier gas flow rate. The  $IrO_2$  particles, attached by electrophoretic deposition cause the cathodic shift in the photocurrent (blue curve) and correcting for the IR losses in the system (ca.  $60 \Omega$ ) gave the final result (green curve).

This work represented a new benchmark for the performance of  $Fe_2O_3$  for PEC water splitting and was published recently in *Angew. Chem. Int. Ed.*<sup>6</sup> In addition, this work was highlighted in the top-tier journal *Nature*.<sup>7</sup>

## Surface Treatments

The first attempts at surface passivation were performed using titanium dioxide and aluminum oxide overlayers deposited by atomic layer deposition (ALD), a technique by which it is possible to deposit conformal films with an atomic thickness resolution. While  $\text{TiO}_2$  overlayers showed no beneficial effect, we found that an ultra-thin coating of  $\text{Al}_2\text{O}_3$  reduced the overpotential required for the state-of-the-art nanostructured photoanodes by as much as 100 mV and increased the photocurrent by a factor of 3.5 (from  $0.24 \text{ mA cm}^{-2}$  to  $0.85 \text{ mA cm}^{-2}$ ) at +1.0 V vs. the reversible hydrogen electrode (RHE) under standard illumination conditions. The subsequent addition of  $\text{Co}^{2+}$  ions as a catalyst further decreased the overpotential and led to a record photocurrent density at 0.9 V vs. RHE ( $0.42 \text{ mA cm}^{-2}$ ). Continued work has led to additional material insights, in particular an electrochemical impedance spectroscopy (Mott Schottky) study was published.<sup>8</sup> In brief, we examined different models used to fit electrochemical impedance data and chose the appropriate one for our nanostructured hematite electrodes. We found that applying this model to our data revealed a drastic change in the charge distribution at the semiconductor liquid junction, upon passivating the surface with  $\text{Al}_2\text{O}_3$  by atomic layer deposition. The Mott Schottky analysis showed that this was not due to a change in the flat band potential of the electrode, which confirmed that the  $\text{Al}_2\text{O}_3$  passivated surface states and that electrochemical impedance spectroscopy could describe the charge transport/transfer in hematite photoanodes with great detail.

Both aluminum oxide and iron oxide sharing the same corundum structure, we decided to test other 13-group metals presenting the same oxide structure. In addition, a less expensive and more scalable application method, chemical bath deposition, was investigated. It has been shown that, as expected, both  $\text{Ga}_2\text{O}_3$  and  $\text{In}_2\text{O}_3$  were sharing the same healing properties as  $\text{Al}_2\text{O}_3$ . Gallium oxide turned out to have even better of an effect and a reduction of overpotential of up to 200 mV was observed. However, the latter material required a higher annealing temperature that is detrimental to the fine structure of the APCVD photoanodes. This important study led to the publication of an article in the journal *Energy & Environmental Science*.<sup>9</sup> The further application of these materials on APCVD prepared samples and the use of atomic layer deposition provided us with a versatile and simple tool to overcome one of the major drawbacks of iron oxide.

### Report on p-doping of $\text{Fe}_2\text{O}_3$ (**Deliverable 17**)

Recently it is been reported that doping of hematite with isoelectronic atoms with smaller ionic radii can decrease the unit cell volume in hematite. This contraction of the unit cell is expected to increase light absorption (via a smaller optical cross section) and increase charge carrier conductivity (via better orbital overlap) and thus increase the performance of hematite photoanodes.<sup>10</sup> We chose to investigate this in our hematite photoelectrodes. Unfortunately attempts to include Al doping in our state of the art APCVD films were not possible due to the inability to identify a suitably volatile and stable metal organic precursor for Al. Thus we attempted to incorporate Al dopant into  $\text{Fe}_2\text{O}_3$  prepared by the spray pyrolysis route. Films were prepared in the standard way<sup>11</sup> and by adding a controlled amount of  $\text{Al}(\text{OAc})_3$  (reported as at% Al based on total metal atoms). The result of the water photo oxidizing performance of the photoanodes with varying amounts of Al dopant is shown in Figure 2 for as-prepared films and for films after annealing at  $550^\circ\text{C}$  for 2 hours.

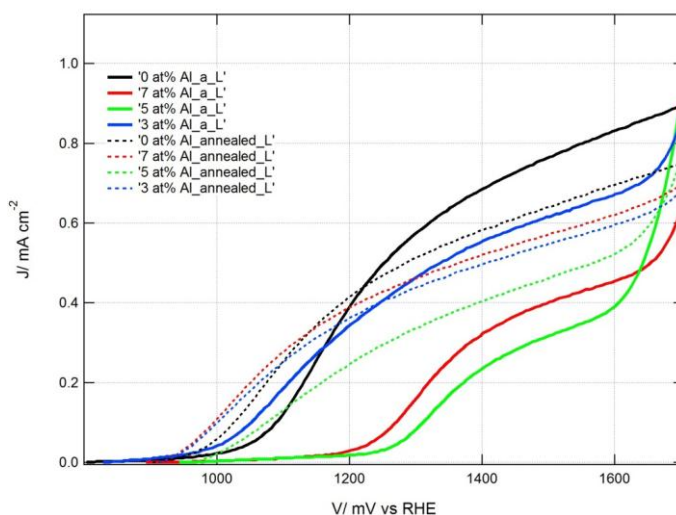


**Figure 2.** Photocurrent vs. voltage curves for  $\text{Fe}_2\text{O}_3$  photoanodes prepared with varying amounts of Al dopant. The solid curves represent the as-prepared films and the dashed curves represent the annealed films ( $550^\circ\text{C}$  for 2 hours).

The Al dopant clearly had a negative effect on the performance of the photoanodes. The performance was equalized after annealing. In addition, no increase in optical absorption was observed (Figure 3). This result gives no indication that Al doping is beneficial for the performance of our Fe<sub>2</sub>O<sub>3</sub> films.

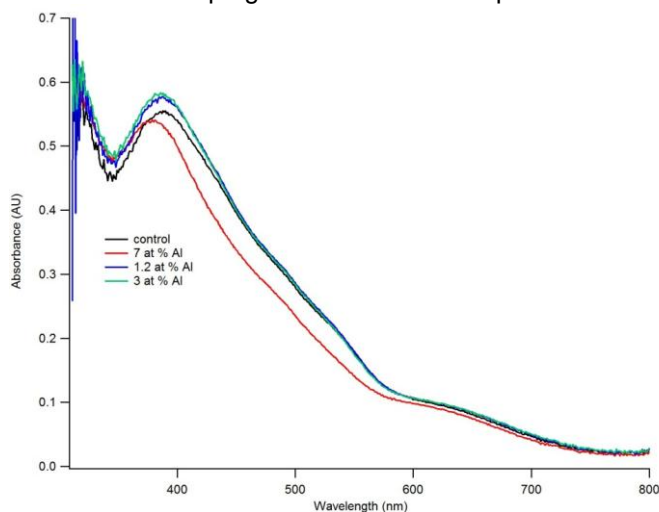


**Figure 3.** UV-Vis absorption (not corrected for reflection) of the Fe<sub>2</sub>O<sub>3</sub> films with varying amounts of Al dopant.

#### *Colloidal Hematite Photoanodes*

We have achieved a new world record in terms of photocurrent at AM 1.5 with  $>4 \text{ mA cm}^{-2}$  (Figure 4). Colloidal nanoparticles were suspended in a paste and doctor-bladed on FTO to afford thin films. After annealing and treating the surface with XXX by ALD, we broke the  $4 \text{ mA cm}^{-2}$  barrier at high overpotentials. Work is in progress to shift this curve to the left (reduce the overpotential). A publication is in preparation.

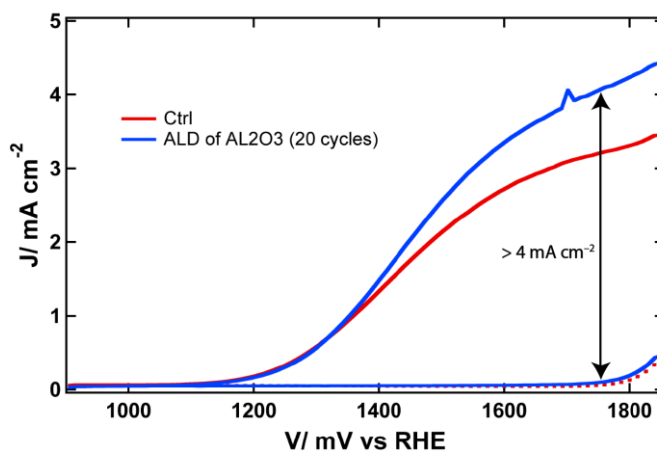


**Figure 4.** Colloidal nanostructured hematite with “healed” surface by ALD aluminum oxide gives greater than  $4 \text{ mA cm}^{-2}$  photocurrent density.

#### **WP-2: Ordered mesoporous oxides as Precursors or Hosts for New Semiconductor Photoanodes**

In 2011 our work in WP2 was divided into two parts corresponding to two distinct goals: the demonstration and development of host/guest photoanodes for water splitting, and the development of new oxides for water splitting.

##### *Host guest photoanodes*

One of the fundamental challenges to using hematite to achieve water splitting with high external quantum efficiency (EQE) is the disparity between the long photon absorption length (hundreds of nm) and the short hole diffusion length (2-4 nm). There are many examples of nanostructure based

approaches that have had some success at improving this situation by decreasing the necessary diffusion length for holes to reach the semiconductor-liquid junction (SCLJ). However, most such reported approaches are based upon high surface area morphologies of pure iron oxide. The concomitant poor electrical properties of hematite homostructures are far from ideal and lead to significant electrical losses. In 2009 a milestone was reached upon the demonstration of the host-guest approach for hematite photoanodes.<sup>12</sup> However, we found that the system was limited by the photo inactive dead layer at the host-guest interface, and only a 60 nm thick film of hematite could be used for good photocurrent. At the end of 2009 we reported the surprising effect of a buffer layer at the interface, made by a treatment with tetraethoxy silicate (TEOS). This buffer layer was found to greatly enhance the performance of the thinnest  $\text{Fe}_2\text{O}_3$  films—a critical aspect for enabling the host guest approach. We then completed a thorough study of this system, which was published in the journal *Advanced Functional Materials*,<sup>11</sup> where it received an “Advances in Advance” article award. In this study, we showed a clear improvement of photoactivity in ultra-thin hematite films for solar water-splitting using a pretreatment of the FTO/glass substrate. A hematite electrode prepared by the spray pyrolysis of  $\text{Fe}(\text{acac})_3$  on a pretreated substrate with an amount of  $\text{Fe}_2\text{O}_3$  equivalent to a 12.5 nm conformal layer (and absorbing only 25% of the incident light at its absorbance maximum,  $\lambda_{\text{max}} = 400$  nm) exhibited a photo-current onset potential at 1.07 V vs RHE and a plateau current of  $0.55 \text{ mA cm}^{-2}$  at 1.43 V vs. RHE, with 30% APCE at 350 nm at 1.43 V. In contrast, almost no photo-activity was observed for the photoanode with the same amount of hematite on an untreated FTO substrate. The pretreatment, consisting of spraying TEOS at high temperature on the substrate surface, was shown to result in the formation of approximately a monolayer of  $\text{SiO}_x$  on the FTO. The iron oxide thin films, analyzed by XRD and transient photo-potentiometry (see Figure 5, Left), showed a better crystallinity and less trapping states when sprayed onto a TEOS pretreated substrate. The morphological analysis of these thin films suggests that the difference is due to separate film formation processes: a Franck-van der Merwe growth (full layer covering the substrate) on  $\text{SiO}_x$  modified substrate against a Volmer-Weber growth mode (island formation) on bare FTO substrate (See Figure 5, Right). This difference reasonably results from a difference in surface energy, perhaps due to the amorphous  $\text{SiO}_x$  layer acting as a lattice strain buffer.

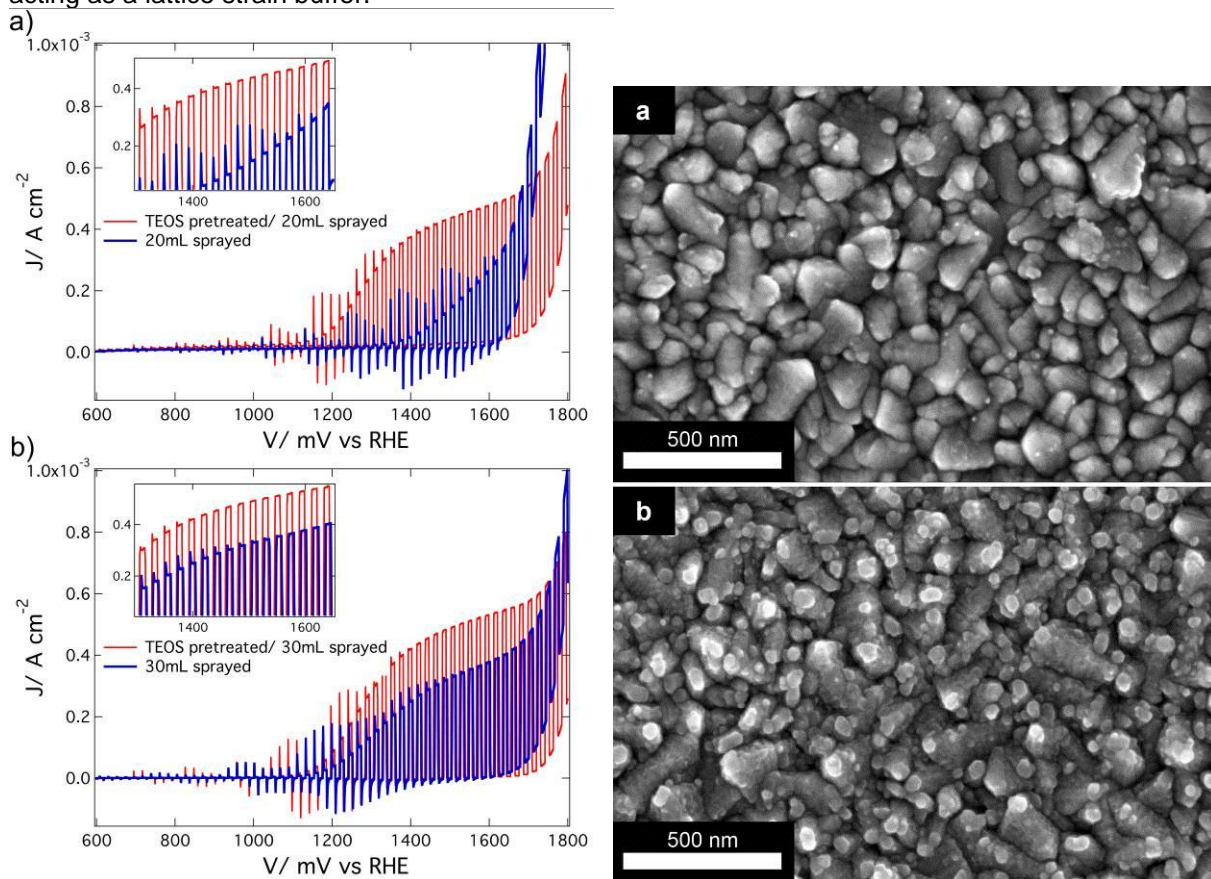


**Figure 5.** Left: Transient photo-response shown by light chopping current densities  $J$  (light on/light off) as a function of the applied potential  $V$ , with respect to the reversible hydrogen electrode (RHE). Comparison of the transient behavior of iron oxide photoanodes using a  $\text{SiO}_x/\text{FTO}$  substrate (red, thin line) and a control FTO substrate (blue, thick line) for the (a) 12.5 nm and the (b) 22 nm  $\text{Fe}_2\text{O}_3$  films. Inset graphs show magnified views of the 1300–1650 mV region for both spectra. Right: SEM images of the  $\text{Fe}_2\text{O}_3$  thin films after 30 mL of the spray solution was deposited on (a) the TEOS treated substrate and (b) the untreated substrate. The beginning of island formation and Stranski-Krastanov can be seen in (a).

With these results we concluded that the crystalline organization was affected by the film nucleation and growth, and is a critical parameter for the photo-activity of ultra-thin hematite films. This study has significantly contributed to a better understanding of the role of iron oxide crystallinity and hematite surface quality on the photo-activity of this promising material for solar energy conversion and storage as hydrogen. Importantly, we can further conclude that it is unlikely an intrinsic limitation exists with hematite ultra-thin films, as previously suggested. As such, further study will continue to focus on very thin film electrodes of hematite including doping and other under-layers in order successfully realize this material in a host-scaffold/guest-absorber approach.

We have also developed a transparent conducting support material with high surface area. The hematite films deposited on these supports have both short hole diffusion lengths to the SCLJ as well as short electron paths to the conducting support. Thus, the host-guest type structures enable the use of many thin films, each having a high IQE, to result in a PEC device with enhanced overall efficiency. Towards this end we have developed niobium doped tin oxide scaffolds produced by atomic layer deposition (ALD) upon macroporous templates. Iron oxide is subsequently deposited on this scaffold by a further ALD process. Thus far we have demonstrated more than twice the photocurrent achievable ( $1 \text{ mA/cm}^2$  at  $1.6 \text{ V RHE}$ ) with analogous monolayer films. This demonstrates the proof of concept that such multilayer composites can significantly enhance the photocurrent. We anticipate additional improvement upon this performance with further optimization, particularly by tuning the interface between the support and hematite combined with hematite doping.

### New oxide electrodes

Cuprous oxide is an abundant and cost-effective p-type semiconductor, which is of great potential for photoelectrochemical hydrogen production due to its low band gap which allows visible light absorption (theoretical maximum of photocurrent of  $15\text{-}18 \text{ mA cm}^{-2}$ ) and favourable conduction band position, cathodic of the hydrogen evolution potential. However, to be used as a photocathode for water reduction this semiconductor needs to be stabilized against photocathodic decomposition.

We have recently shown that protection of  $\text{Cu}_2\text{O}$  can be achieved by atomic layer deposition (ALD) of ultrathin films of Al:ZnO and  $\text{TiO}_2$ .<sup>13</sup> ZnO assists in the electron extraction from  $\text{Cu}_2\text{O}$  and also provides a better surface for  $\text{TiO}_2$  film nucleation during ALD growth. In turn,  $\text{TiO}_2$  acts as an effective barrier layer, preventing the dissolution of ZnO in acidic aqueous environments. Photocurrents as high as  $7 \text{ mA cm}^{-2}$  were observed under AM 1.5 illumination for  $\text{Cu}_2\text{O}/\text{Al:ZnO}(20 \text{ nm})/\text{TiO}_2(10 \text{ nm})/\text{Pt}$  electrodes. During stability test at  $0 \text{ V/RHE}$  the photocurrent gradually decayed despite the chemical stability of  $\text{Cu}_2\text{O}$  during the photoelectrochemical measurements.

The as-deposited  $\text{Cu}_2\text{O}$  films obtained by galvanostatic electrodeposition at pH 12 in optimized conditions have been deeply investigated by photoelectrochemistry, electrochemical impedance, UV-visible spectroscopy and Terahertz pump-probe spectroscopy, in order to adjust the film thickness to the optical and electrical properties of the semiconductor. The capacitance measurements carried out in sodium acetate in the potential range where stability is predicted by the Pourbaix diagram show a flat band potential of  $+(0.75\pm 0.05)\text{V}$  vs. RHE, therefore a conduction band position of about  $-1.0 \text{ V/RHE}$  calculated on the basis of the  $2.0\text{-eV}$  band gap and the donor density. Therefore, the semiconductor is more than capable of efficient water reduction (Figure 6).

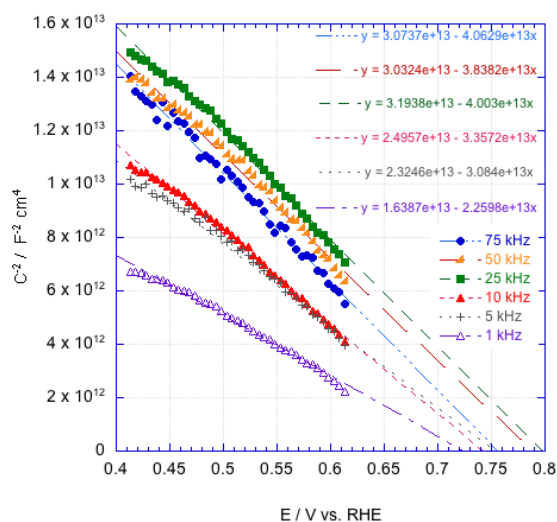


**Figure 6.** Mott-Schottky plots obtained by fitting the capacitance data in the range 50KHz-0.5Hz for  $\text{Cu}_2\text{O}$  in 0.1M sodium acetate.

The absorption coefficient obtained from the transmittance and reflectance of Cu<sub>2</sub>O deposited on conductive glass shows that the optical penetration depth at 550 nm is about 1 μm (Figure 7). Therefore gold, which reflects light for λ > 550 nm, is a convenient substrate to decrease the film thickness and reduce the film resistance. The morphology of the electrodeposited Cu<sub>2</sub>O shows corners of cubic crystals about 500 nm-large, which is likely to exceed the photogenerated electrons lifetime. The electrodeposition parameters (temperature, current of deposition, pH) were also varied in order to decrease the crystal size but no photocurrent gain was recorded.

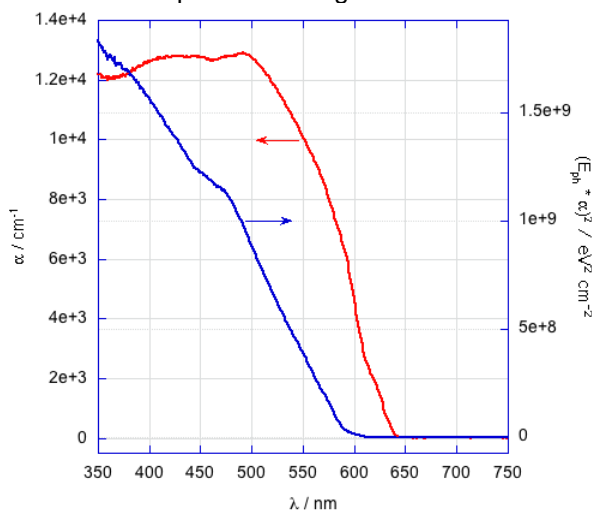


**Figure 7.** Absorption coefficient and Tauc plot for the electrodeposited Cu<sub>2</sub>O film.

The photoconductivity dynamics were probed by THz spectroscopy, by measuring the photoconductivity as a function of pump-probe delay time for excitation at 600 nm. The resulting electron mobility and diffusion length were calculated 2.4 cm<sup>2</sup>/Vs and 30 nm, respectively. This measurement seems to indicate that structuring of the Cu<sub>2</sub>O would be beneficial for improving the light-to-current efficiency.

The mechanism of photocurrent decay in Cu<sub>2</sub>O/AZO/TiO<sub>2</sub>/Pt electrodes has been previously explained by the formation of Ti<sup>3+</sup> states in the top titania film, as assessed by XPS before and after PEC. Electron trapping in the TiO<sub>2</sub> finally promotes TiO<sub>2</sub> dissolution and photocathode failure. Considerable progress has been made in the stabilization of the photocathodes by depositing TiO<sub>2</sub> at higher temperatures. Amorphous layers of Al:ZnO and TiO<sub>2</sub> can be stable for more than one hour in Na<sub>2</sub>SO<sub>4</sub> 0.5 M, KPi 0.1 M electrolyte (pH 5, Figure 8). The total time of measuring was 3 hours and the photocurrent decayed to 80% of the initial value (not shown).

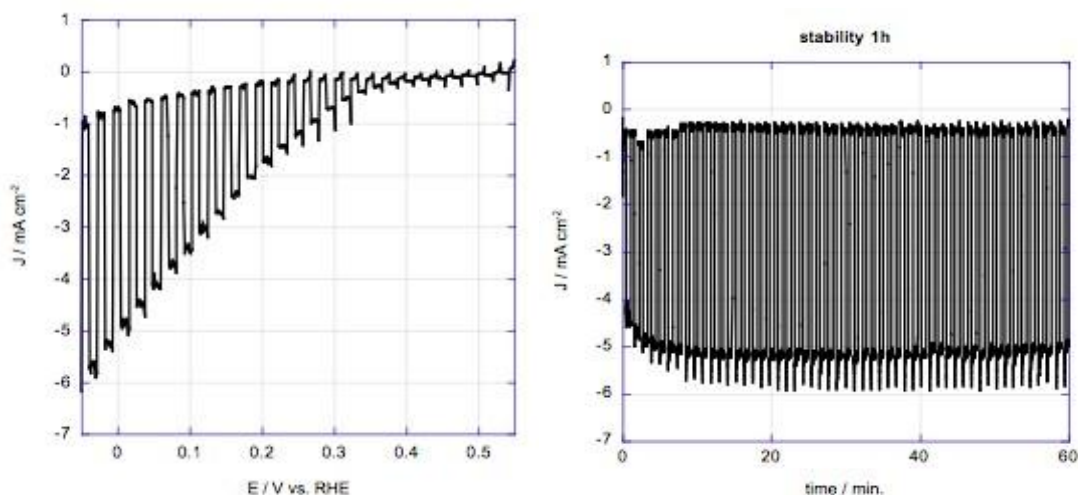


**Figure 8.** Linear sweep and photocurrent at 0V/RHE under chopped AM 1.5 illumination in Na<sub>2</sub>SO<sub>4</sub> 0.5 M purged with N<sub>2</sub>.

The photocurrent stability seems to be very sensitive to the temperature at which ALD TiO<sub>2</sub> is grown. The data shown in Figure 8 are for Al:ZnO deposited at 120°C and TiO<sub>2</sub> deposited at 150°C. The same batch of Cu<sub>2</sub>O protected with Al:ZnO and TiO<sub>2</sub> grown at 120°C was not as stable, although more photoactive (7 mA cm<sup>-2</sup> at 0V/RHE), and the photocurrent after 1 hour equalled only 25% of the initial value. Based on the ellipsometry results on Si wafer, the growth rate is slowed down from 0.66 Å/cycle to 0.054 Å/cycle for a deposition at 120°C and at 150°C, respectively, which is unusual for

ALD and might indicate that the film structure is more compact. Insertion of layers of Nb in TiO<sub>2</sub> with a spacing of 1-1.3 nm, improved stability when the ALD TiO<sub>2</sub> was deposited at 120°C (70-85 % of the initial photocurrent after 60 minutes) but not significantly at 150°C. Pentavalent Nb dopant might favour a more compact structure by creating Ti interstitials, which could explain the increased stability. A more compact structure is expected to increase the chemical stability of the amorphous TiO<sub>2</sub> at acidic pH, in analogy to the higher chemical stability showed by TiO<sub>2</sub> crystallized in the rutile phase than in the anatase phase. Moreover, we have found that ALD TiO<sub>2</sub> deposited at 120°C has a more anodic Fermi level position (+250 mV/RHE) compared to ALD TiO<sub>2</sub> 150°C (-50 mV/RHE), as measured by electrochemical impedance on 50-nm thick films deposited on conductive glass. Electron injection in the electrolyte is therefore favoured for the TiO<sub>2</sub> grown at higher temperature, and consequently Ti<sup>3+</sup> states formation is reduced and chemical stability increased.

Different mechanisms can be at the origin of the protective layer instability:

1. TiO<sub>2</sub> dissolution via preliminary reduction, with consequent electrode failure.
2. Drop of the local pH close to the electrode surface during H<sub>2</sub> evolution and pitting corrosion of TiO<sub>2</sub>.
3. Partial TiO<sub>2</sub> dissolution until the equilibrium concentration is reached with the electrolyte. In this case, the inconvenience is caused by the removal of the Pt catalyst
4. Pt catalyst instability due to poor adhesion of the electrochemically deposited particles.

The first issue can be solved by increasing the Fermi level position in titania, such that electron injection is not hindered. This has been done both by partially replacing Ti<sup>4+</sup> with Nb<sup>5+</sup> and by depositing at higher temperature. Although the results are a considerable progress, a very long-term stability has not been attained yet and ALD of such thin films is affected by a certain lack of reproducibility.

The second issue has been addressed by increasing the buffer capacity of the electrolyte and replacing Na<sub>2</sub>SO<sub>4</sub> 0.5 M, KPi 0.1 M with 1 M acetate (pH 5), or 1 M phosphate (pH 7) or 1 M borate (pH 9). At basic pH the photoactivity was reduced without any improvement in the stability of the photocurrent under continuous or chopped illumination. At lower pH (H<sub>2</sub>SO<sub>4</sub> 0.1 M, pH 1), the photocurrents were very high but the electrode failure considerably accelerated. pH 5 seems to be the optimal choice for this system but a considerable difference was found in the stability in presence or absence of acetate, as shown in Figure 9. For this study the protective layer deposited directly on conductive glass and the electrodes dipped for 12 or 24 hours in the electrolyte. If the protective layer is continuous it should act as a blocking layer in the presence of Fe<sup>2+</sup>(CN)<sub>6</sub>/Fe<sup>3+</sup>(CN)<sub>6</sub> redox couple. While the CV does not show any redox peak after dipping in Na<sub>2</sub>SO<sub>4</sub> 0.5 M, KPi 0.1 M, the film was no more continuous after dipping in acetate 1 M. Therefore, in order to solve the diffusion problem in the electrolyte and use a concentrated buffer at pH 5, such as acetate, TiO<sub>2</sub> need to be crystallized.

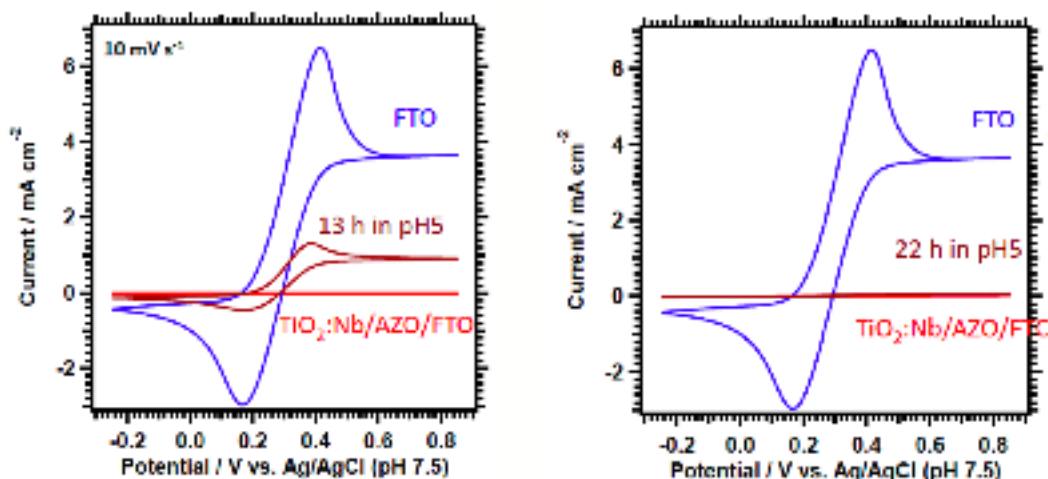


**Figure 9.** CV in presence of Fe<sup>2+</sup>(CN)<sub>6</sub>/Fe<sup>3+</sup>(CN)<sub>6</sub> redox couple for as deposited TiO<sub>2</sub> (left) and exposed to 200°C and oxygen for 2 hours (right).

Mechanism 4, including Pt poisoning and de-activation, seems to be proved by the effect of subsequent platinizations, after which the initial photocurrent is recovered (Figure 10).

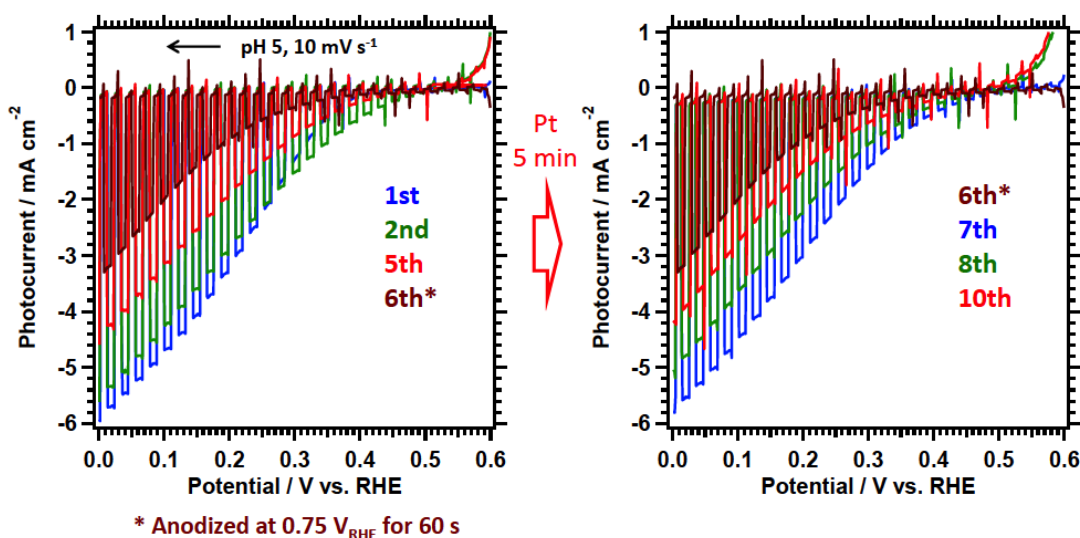


**Figure 10.** Subsequent potential sweeps showing progressive photocurrent reduction but recovering after a new platinization.

The mechanism was studied on bare FTO by following the same procedure as for the actual photocathodes and electrochemically depositing the Pt catalyst from  $\text{H}_2\text{PtCl}_6$  1 mM. By applying a potential negative of the HER, the dark current is flat and stable for at least one hour. Platinum seems to be stable in the dark, therefore the origin of instability might be sought in the mechanism 3. In order to stabilize the protective layer against dissolution, the  $\text{TiO}_2$  crystallinity should be increased by thermal treatments after ALD or the  $\text{TiO}_2$  should be replaced or covered with another layer. Oxides with suitable conduction band position such as  $\text{Ga}_2\text{O}_3$ ,  $\text{Nb}_2\text{O}_5$ ,  $\text{In}_2\text{O}_3$  and  $\text{SnO}_2$  were either not stable ( $\text{Nb}_2\text{O}_5$ ,  $\text{In}_2\text{O}_3$  and  $\text{SnO}_2$ ) or too insulating ( $\text{Ga}_2\text{O}_3$ ) for the minimal thickness required for complete coverage.

The growth temperature of ALD  $\text{TiO}_2$  and the degree of initial disorder decide for whether or not a film as thin as 10-20 nm can become partially or completely crystalline after annealing. We have found that post-anneal of  $\text{TiO}_2$  grown at 150°C does not lead to any crystalline fraction below a certain thickness and also the strain due to crystallization of less than 10 nm-films induces cracks in the protective layer. Films deposited at 200°C can actually be partially crystallized with a post-treatment at 200°C for few hours. The broadening of the XRD peaks, with HWFM as wide as 2-2.5°, indicates a considerable strain in the film.

A mild annealing of  $\text{Cu}_2\text{O}$  at 250°C in Ar before ALD does not alter the morphology or cause any loss of photoactivity (Figure 11). Annealing the electrode after ALD at the same temperature improves the crystalline fraction in the overlayers but strains considerably the structure, increasing recombination of the photogenerated carriers and photocurrent drop.

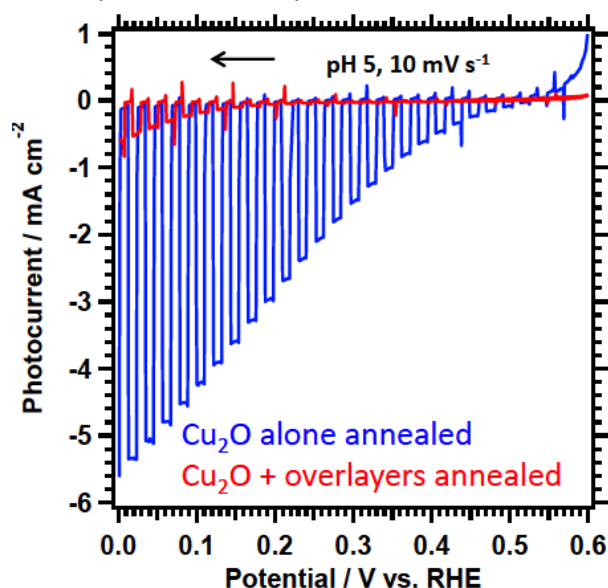


**Figure 11.** Linear sweeps showing the effect of heat treatment at 250°C in Ar for  $\text{Cu}_2\text{O}/\text{Al}:\text{ZnO}$  (10 nm)/ $\text{TiO}_2$  (10 nm)/Pt.

Increasing the thickness above 15 nm causes a significant potential shift to more negative potentials (Figure 12), which might be explained by the lesser cathodic Fermi level potential in  $\text{Cu}_2\text{O}$  with increasing thickness of the n-type semiconductors.

In conclusion, the mechanisms of photocurrent decay under operating conditions has not been understood yet. Studies are still ongoing in order to find out if the photocurrent decay is simply due to platinum de-activation when the electrode is both exposed to light and biased at 0V/RHE or if there is a progressive degradation of the protective layer under operating conditions, which would be solved by an optimal ALD protective layer/electrolyte system

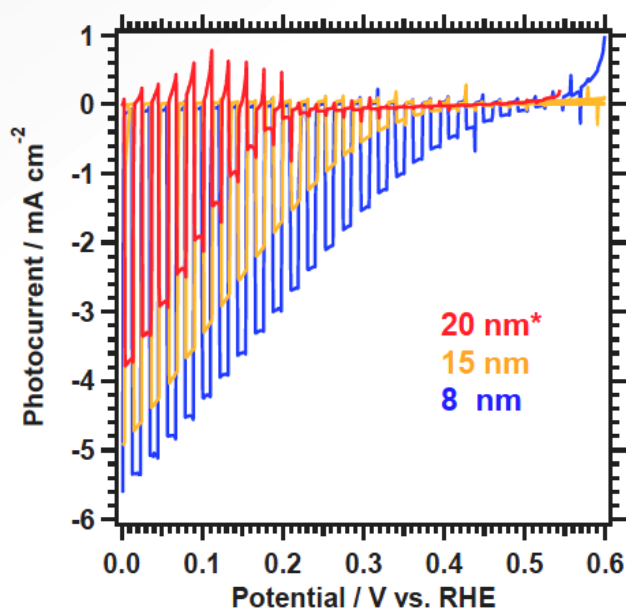


**Figure 12.** Linear sweep curves in chopped illumination for different  $\text{TiO}_2$  thickness in the electrode.

## Évaluation de l'année 2011 et perspectives pour le prochain projet

### WP-1: $\alpha\text{-Fe}_2\text{O}_3$ photoanodes

The PECHouse project has brought landmark advancement to the  $\alpha\text{-Fe}_2\text{O}_3$  photoanodes prepared by APCVD. We continue to enhance the performance and increase the understanding of this promising system for PEC hydrogen production. Our unmatched performance benchmark with hematite photoanodes was honored with a highlight in the top scientific journal, *Nature*. We are very close to meeting the final project deliverable and milestone of  $5 \text{ mA cm}^{-2}$  with this material by the end of 2011 (with our  $>4 \text{ mA cm}^{-2}$  of photocurrent given by the colloidal samples) and we are on track to produce a system that can convert sunlight and water into hydrogen at a price of  $5\text{€}/\text{kg H}_2$  by 2015 (see Figure 13). The most critical area which needs to be improved is the overpotential. Our work in the future will focus on understanding the limitations at the surface that result in the high overpotential, as well as further increasing the photocurrent of the hematite photoanodes. The former point will be accomplished by first assessing the surface vs. bulk recombination, and by continuing to investigate surface passivation techniques.

Our state-of-the-art  $\text{Fe}_2\text{O}_3$  photoanodes surpass the performance of any other inexpensive oxide-based PEC system by producing 4.8% STH conversion efficiency in a tandem cell configuration with 2 DSCs. To meet the EU projected cost of  $5\text{€}/\text{kg H}_2$  by 2015 the STH conversion efficiency should be increased to 10%—corresponding to a photocurrent of about  $7 \text{ mA cm}^{-2}$ . Figure 13 shows the progress of the photocurrent at PECHouse. The goal of  $7 \text{ mA cm}^{-2}$  can be reasonably reached by 2015.

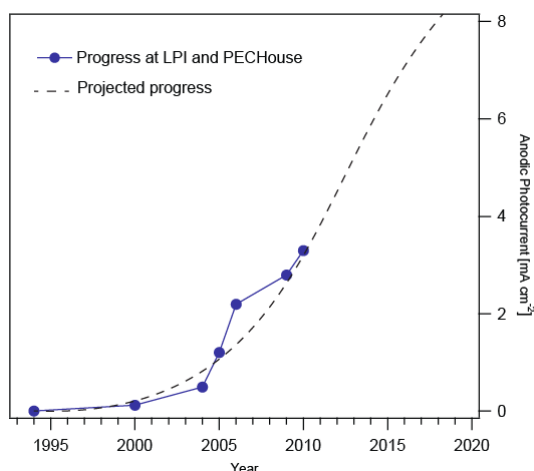


**Figure 13.** Progress at EPFL of the photocurrent density (at 1.23 V vs. RHE under standard testing conditions) of the state-of-the-art Fe<sub>2</sub>O<sub>3</sub> photoanodes is shown with a projection. The projection suggests that the benchmark photocurrent density of 7 mA cm<sup>-2</sup> will be achieved by 2015.

## WP-2: Host-guest system and New Semiconductor Photoanodes

Considerable progress has been achieved in 2011 in WP2. New underlayers have been evaluated and were found to be superior to the previous most promising host-guest system: FTO/SiO<sub>x</sub>/Fe<sub>2</sub>O<sub>3</sub>. In order to advance the photocurrent delivered by these systems, the host material will have to be sufficiently structured. Our current efforts are in collaboration with Prof. Ozin's group (Toronto) in preparing inverse opal-like electrodes of ATO (Sb:SnO<sub>2</sub>) as this is similar to FTO there should be no issues with applying the buffer layer and the Fe<sub>2</sub>O<sub>3</sub>. However, a suitable deposition method for the Fe<sub>2</sub>O<sub>3</sub> must be developed. We are currently trying to conformally deposit Fe<sub>2</sub>O<sub>3</sub> by ALD to demonstrate high photocurrents with the host guest approach. We have also made important advances in niobium-doped SnO<sub>2</sub> nanostructures as a host material. In addition, in only two years working on Cu<sub>2</sub>O photocathodes we achieved breakthrough results in stability and photocurrent densities. The parameter space has been diligently assessed and a follow up publication to our *Nature Materials* paper is in preparation. Importantly, **the overall project milestone and deliverable of 5 mA cm<sup>-2</sup> has been vastly exceeded with this material (demonstrated > 7 mA cm<sup>-2</sup>).**

## Références

1. Bjorksten, U.; Moser, J.; Gratzel, M. *Chem. Mater.* **1994**, *6*, 858-863.
2. Duret, A.; Gratzel, M. *J. Phys. Chem. B* **2005**, *109*, 17184-17191.
3. Cesar, I.; Kay, A.; Martinez, J. A. G.; Gratzel, M. *J. Am. Chem. Soc.* **2006**, *128*, 4582-4583.
4. Kay, A.; Cesar, I.; Gratzel, M. *J. Am. Chem. Soc.* **2006**, *128*, 15714-15721.
5. Cornuz, M.; Grätzel, M.; Sivula, K. *Chemical Vapor Deposition* **2010**, *16*, 291.
6. Tilley, S.; Cornuz, M.; Sivula, K.; Grätzel, M. *Angew. Chem. Int. Ed.* **2010**, *49*, 6405-6408.
7. *Nature* **2010**, *466*, 669-669.
8. Le Formal, F.; Tetreault, N.; Cornuz, M.; Moehl, T.; Gratzel, M.; Sivula, K. *Chem. Sci.* **2011**.
9. Hisatomi, T.; Le Formal, F.; Cornuz, M.; Brillet, J.; Tetreault, N.; Sivula, K.; Gratzel, M. *Energy & Environmental Science* **2011**, *4*, 2512.
10. A. Kleiman-Shwarsstein, M. N. Huda, A. Walsh, Y. F. Yan, G. D. Stucky, Y. S. Hu, M. M. Al-Jassim and E. W. McFarland, *Chem. Mater.*, 2010, **22**, 510-517.
11. Le Formal, F.; Grätzel, M.; Sivula, K. *Adv. Funct. Mater.* **2010**, *20*, 1099-1107.
12. Sivula, K.; Le Formal, F.; Gratzel, M. *Chem. Mater.* **2009**, *21*, 2862-2867.
13. Paracchino, A.; Laporte, V.; Sivula, K.; Grätzel, M.; Thimsen, E., *Nature Materials* **2011**, *10* (6), 456-461.